Presented at the 36th European PV Solar Energy Conference and Exhibition, 9-13 September 2019, Marseille, France

NON-DESTRUCTIVE APPROACH FOR MEASURING BASE RESISTIVITY OF EMITTER-DIFFUSED, PARTIALLY-PROCESSED WAFERS USING TEMPERATURE-STAGE QSSPC

V. Kuruganti, J. Haunschild, A. Brand, S. Al-Hajjawi, S. Rein
Fraunhofer Institute for Solar Energy Systems ISE, Heidenhofstraße 2, 79110 Freiburg, Germany
Telephone: +49 761 4588 5736, e-mail: vaibhav.kuruganti@ise.fraunhofer.de

ABSTRACT: A novel non-destructive and contactless approach for measuring the base resistivity of emitter-diffused, partially-processed wafers is introduced. The method is based on temperature-dependent resistivity analysis and referred as temperature-dependent resistivity slope model (TRSM). It is developed for p-type boron-doped silicon wafers used in industrial applications with base resistivities ranging from 1 to 5 Ωcm. A sensitivity analysis is carried out on TRSM to determine the limits of this simple approach and the results show that TRSM can determine the base resistivity with an accuracy of 90%. The main limiting factor is the reproducibility from the measuring tool with a mean error of 6% on the TRSM results. Finally, the base resistivity of emitter-diffused, partially-processed wafers (in this work referred as precursor wafers) obtained from TRSM is compared to two reference approaches and showed mean error percentages of less than 10%.

Keywords: Silicon, Characterisation, Passivation and Etching

1 INTRODUCTION

Resistivity is a fundamental property of a material that quantifies how strongly the material resists the flow of electric current. Resistivity serves as an input parameter to find other material properties like doping concentration, mobility [1] etc. In PV industries, most of the precursor wafer suppliers provide wafers with a wide range of base resistivities and knowing the accurate base resistivity of these wafers becomes critical for industrial and research purposes. Analysing the base resistivity is important for quality control at different processing stages of solar cells for example it is necessary to find optimal processing parameters like the pitch of laser contact openings (LCO) at the later processing stages of the solar cell [2] and to determine the presence of electrically active complexes like thermal donors [3].

To measure the resistivity of a wafer, different approaches have been established. Four-point probe (FPP) technique [4] is one of the most successful and widespread techniques used as a standard in the semiconductor industry for determining the resistivity of a wafer. It is an absolute resistivity measurement without recourse to calibrated standards. For an arbitrarily shaped sample and equal spacing between the probe tips, the base resistivity can be expressed as:

$$\rho = \frac{\pi}{\ln 2} * t * \frac{V}{I} \qquad (1)$$

Here, ρ is the resistivity (Ωcm), V the voltage (mV), I the current (mA) and t the thickness of the sample (cm). The Eq. (1) is valid provided the sample thickness is smaller than the spacing of the probe tips. As the probe tips need to touch the sample or even penetrate its surface, resistivity measurements performed with FPP can cause local damages especially to emitter or passivation layers. If both sides of a precursor wafer are measured, base and emitter resistances can be separated. If the coating of the sample is mechanically too strong or thick to be penetrated by the tips, FPP cannot be applied.

Inductive eddy current (EC) resistivity measuring technique [5] is a non-destructive approach. When measuring a precursor wafer, EC technique measures the total sheet resistance (R_T) which is the parallel summation of emitter (R_E) and base sheet resistance (R_B), see Eq. (2). Hence, it becomes impossible to determine the base sheet resistance using only the EC technique for a precursor wafer.

$$\frac{1}{R_T} = \frac{1}{R_E} + \frac{1}{R_B} \qquad (2)$$

A non-destructive approach, which is based on photoluminescence imaging (PLI) and photoconductivity (PC) techniques has already been proposed by Höffler et al. [6]. The PLI–PC approach is a robust method to determine the base resistivity of a precursor wafer with error percentages as low as 10%.

In this work, an alternative non-destructive method referred to as temperature-dependent resistivity slope model (TRSM) is introduced to determine the base resistivity of a precursor wafer using WCT-120TS also called as temperature-stage quasi-steady-state photoconductivity (TS-QSSPC) from the company Sinton Instruments [7]

2 THOERY

Many material properties like resistivity, mobility, and lifetime change with temperature [8]. In order to be able to compare the results, the measurements should always be performed under standard testing conditions (e.g. at 25°C). In this paper, the effect of temperature on base sheet resistance and emitter sheet resistance is studied extensively and using these results, TRSM is developed to determine the base resistivity of a precursor wafer. In order to understand the temperature dependence on emitter sheet resistance and base sheet resistance separately, the mobility model from Dorkel and Leturcq [9] was chosen. Dorkel and Leturcq mobility model describes the effect of doping, injection level and temperature on the overall mobility computation in cogent manner. The reason for choosing Dorkel and Leturcq mobility model as a standard model is because of its simplicity, pragmatic approach, ability to clearly distinguish between lattice scattering [10] and ionic [11] scattering mechanisms and finally the tool used for this

analysis, i.e., WCT-120TS, uses Dorkel and Leturcq as the standard model as well. The Dorkel and Leturcq model contains three dominant scattering mechanisms namely: lattice scattering, impurity scattering and carrier-carrier scattering [12]. Lattice scattering is caused due to the vibration of the lattice atoms and is temperature-dependent. Impurity or ionic scattering is due to the ionic impurity atoms attracting the free charge carriers. Impurity scattering is temperature and doping concentration dependent. Carrier-carrier scattering is due to the collision of free charge carriers and depends on temperature and concentration of electrons and holes. All the above scattering mechanisms are combined to determine the overall mobility. Resistivity is calculated using the overall mobility and doping concentration.

A Dorkel and Leturcq model simulating tool was developed and temperature-dependent resistivity analysis was carried out for typical emitter and base layers used in the photovoltaic industry (Table I).

Table I: Properties of typical emitter and base layers.

	Base	Emitter
Thickness (µm)	180	3
Type of doping	p-type	n-type
Doping concentration (cm^{-3})	10^{15}-10^{16}	10^{18}-10^{19}

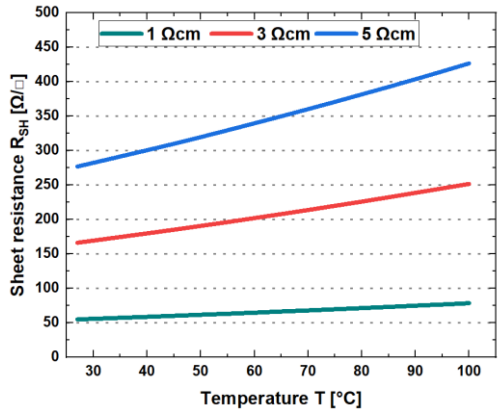

Figure 1: Simulation of the temperature dependence of R_{SH} for typical base resistivities using the Dorkel and Leturcq mobility model.

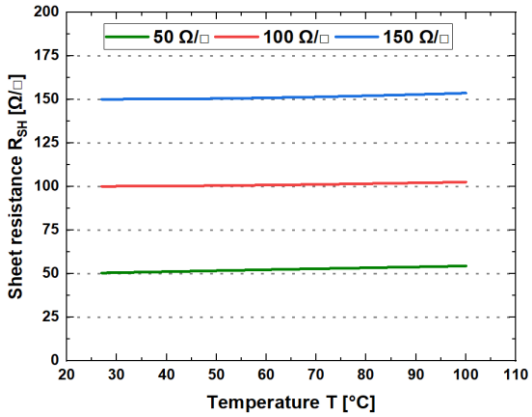

Figure 2: Simulation of the temperature dependence of R_{SH} for typical emitter layers using the Dorkel and Leturcq mobility model.

For typical base resistivities in the range of 1 to 5 Ωcm (Figure 1), we observe a strong temperature dependence and with increase in the base resistivity, we observe that the slope of the curve increases, whereas in the case of the typical emitter layers with sheet resistance ranging from 50 to 150 Ω/□ (Figure 2), only a marginal increase of resistance with respect to temperature is observed.

Clearly, from Figure 1 and Figure 2 the R_{SH} vs. temperature behavior for the emitter and base layer is different. Thickness of the sample or the type of doping cannot explain such differences in temperature vs. R_{SH} results, but doping concentration does. Detailed analysis was carried out to understand the effect of doping concentration on R_{SH} vs. temperature (Figure 3). It is observed that carrier-carrier scattering does not have a significant role. The overall mobility is dominated by lattice mobility at low doping concentration, i.e., typical base layers. At doping concentrations of 10^{17} cm^{-3}, the overall mobility is equally dominated by both, ionic and lattice mobility. At high doping concentration, i.e., typical emitter layer, the overall mobility is dominated by ionic mobility. Hence, because of the different dominant scattering mechanisms, emitter and base layer behave differently with respect to temperature.

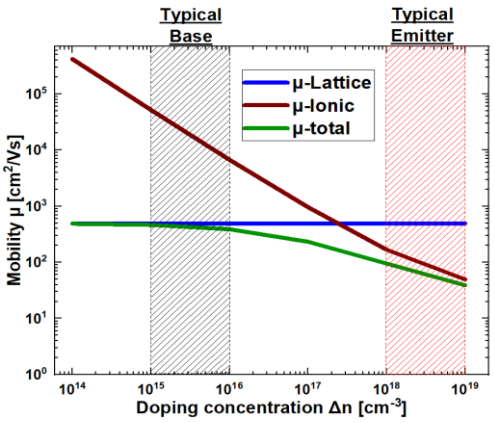

Figure 3: Simulated results of mobility vs. doping concentration using the Dorkel and Leturcq mobility model.

3 TEMPERATURE-DEPENDENT RESISTIVITY SLOPE MODEL (TRSM)

In the previous section, it has been shown that the emitter and base have different temperature vs. R_{SH} behavior. The base layer has a strong temperature dependence whereas in the emitter layer remains almost constant with increase in temperature. Since the total sheet resistance is the parallel summation of emitter and base sheet resistance (Eq. (2)), the lowest resistance among emitter and base dictates the overall sheet resistance. At higher temperatures, the base sheet resistance is very high and hence the overall sheet resistance is closer to the emitter sheet resistance. A theoretical model is developed such that, if the slope of the overall sheet resistance is known at 85 to 90°C, emitter sheet resistance is deduced from it. The range of 85 to 90°C is chosen out of practical reasons from the experimental setup. With the measured data of the total

resistivity and the calculated data of the emitter, the base sheet resistance can be computed.

The first step in the development of our theoretical slopes model (Figure 4) is to simulate the temperature-dependent sheet resistance values of base resistivity ranging from 1 to 5 Ωcm and for 3 emitter layers with sheet resistance of 50, 100 and 150 Ω/□. One emitter sheet resistance is fixed and using all the different base resistivities, temperature-dependent total sheet resistance data is obtained using Eq. (2). The same procedure is implemented for the other emitter layers.

The second step of the model development is to determine the slopes of these base, emitter and total sheet resistances vs. temperature data. The average slope at 85 to 90°C of different total sheet resistances obtained from one emitter and different base resistivities is determined.

In the final step, the average total sheet resistance slope at 85 to 90°C is equated to the emitter sheet resistance and by interpolating the simulated data, a generalized equation is developed using which the emitter sheet resistance can be deduced for a precursor wafer. Base resistivity can be determined using Eq. (2).

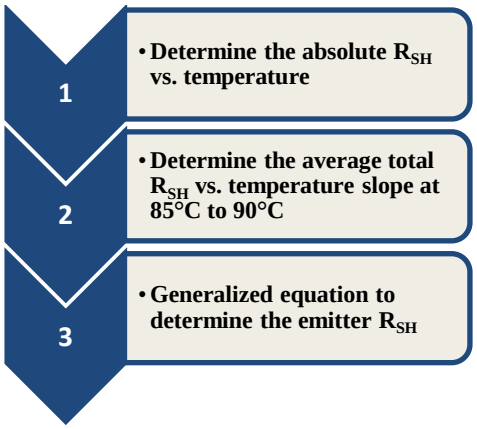

Figure 4: Flowchart of the TRSM approach

The results of the TRSM were validated with the online resistivity simulating tool PV Lighthouse [13] and it was found that the mean error percentage of TRSM is less than 10% for the wafers from the calibration set mentioned above. Sensitivity analysis on TRSM was carried out to investigate the accuracy of the model and to find regions with increased error percentage.

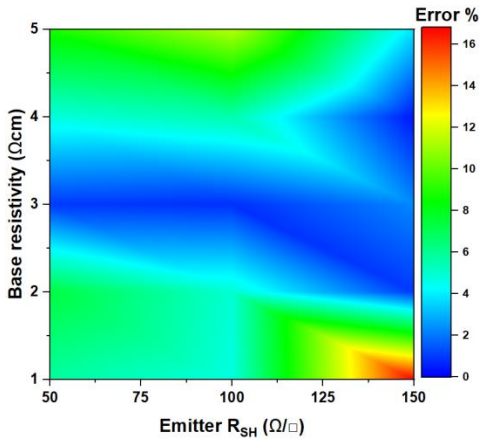

Figure 5: Contour plot of the sensitivity analysis of TRSM

From Figure 5, it can be observed that at low base resistivities and high emitter R_{SH}, the error percentages are very high. The error percentages go up to 17%. During the development of TRSM model step 2 and 3 (Figure 4), the average total R_{SH} slope at 85-90°C is correlated to the emitter sheet resistance. For a given emitter layer the average total sheet resistance lies between base resistivities of 2.5 to 3.5 Ωcm. Hence we observe lower error percentages in the middle region and as we move away from this zone, high error percentages are observed.

4 EXPERIMENTAL PROCEDURE

In order to validate the TRSM, a set of Cz 10 samples with alkaline texture, emitter and rear-side passivation have been selected (Figure 6).

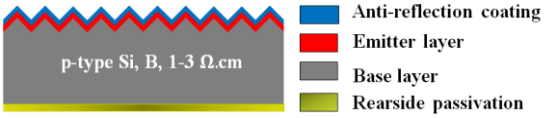

Figure 6: Schematic representation of the typical selected sample

All the selected samples have a lightly p-doped base layer (1-3 Ohm.cm), a highly n-doped emitter layer, and thin antireflection coating (ARC) and rearside passivations. Figure 7 illustrates the various processing steps and measurements performed on the selected sample set.

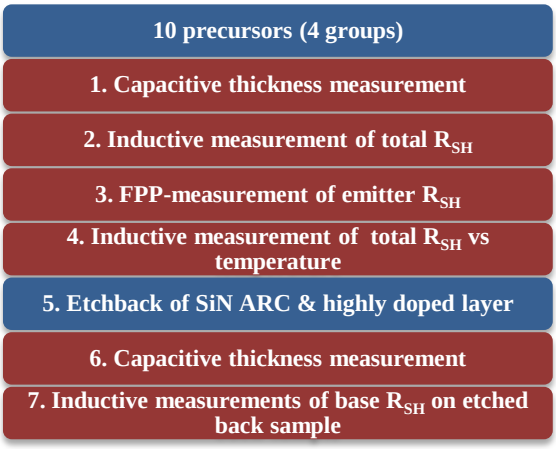

Figure 7: Schematic representation of various processes involved in the experimental procedure

For the selected precursor samples, the thickness is measured capacitively and the total sheet resistance is measured inductively with the commercially available tool MX 152 from the company E+H Metrology [14]. Four-point-probe (FPP) measurements are performed on the front side of the sample to determine the emitter sheet resistance with the commercially available tool FPP-SCAN from the company PV-Tools [15]. The total sheet resistance from MX 152 and the emitter sheet resistance from FPP-SCAN are used to determine the base resistance of the sample and we use it as our first reference value. In this study, this is referred to as "FPP–EC approach". The temperature-dependent measurements

of the total sheet resistance are performed on the commercially available tool WCT-120TS from Sinton Instruments. TRSM is applied to the temperature-dependent total sheet resistance measurement and the base sheet resistance is predicted. The next processing step involves chemical etching, in which the emitter layer and ARC are etched back using chemicals like nitric acid (HNO_3) and hydrofluoric acid (HF). Again the thickness and resistivity are measured with a MX-152. Now, the inductively measured resistivity equals the base resistivity and we have a second reference value for comparison. In this study, it is referred to as "no emitter EC approach".

5 RESULTS

Figure 8 depicts the reproducibility of the slopes at 85 to 90°C for a single sample measured on WCT-120TS tool. It is evident from Figure 8 that the results are not completely constant for the selected sample and this can have a significant effect on the TRSM. TRSM uses the measured slope at 85-90°C and when the slope deviates due to lack of reproducibility, it can negatively influence the computation of base sheet resistance. The effect of instrumental drift from the tool led to a mean error percentage of 6% on the TRSM and hence, it was used as the error bar for TRSM in final comparison (Figure 9).

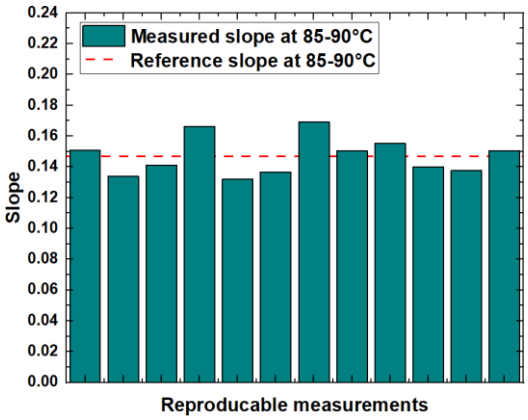

Figure 8: Reproducibility test of the same wafer performed on the temperature-dependent resistivity measuring tool

Figure 9 represents the quantitative comparison of the TRSM with respect to no emitter EC approach and FPP-EC approach. Red triangles represent the comparison of TRSM with respect to no emitter EC approach, blue triangles represent the comparison of TRSM w.r.t FPP-EC approach and the dashed line is the bisecting line. For most of the wafers, the reference values are met within the accuracy of the method. Certain differences are observed in the two reference values for the base resistivity (less than 5 %) and this can be because of different characterizing techniques and the lack of reproducibility of the measuring tools. From Korsós et al. [16], it has been observed that measuring the emitter R_{SH} of a precursor wafer by means of FPP approach is highly dependent on the surface properties of the passivation layer. If we have a rough surface, then no good contact between the measuring tips and the wafer surface can be made. It was observed that single FPP measurement always had lower emitter R_{SH} values and several subsequent measurements at the same point have increased the measured emitter R_{SH} to the reference values due to better contacting between the measuring tip and the wafer emitter surface. In this paper single FPP measurements were performed on the emitter layer and hence lower emitter R_{SH} is measured. Since lower emitter sheet resistance is measured, we observe overestimation of the base resistivity (Figure 9) using FPP-EC approach incomparison to no emitter EC approach.

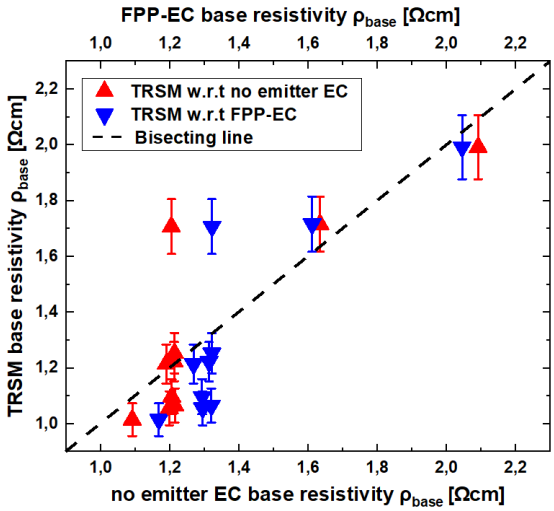

Figure 9: Comparison of predicted base resistivity from TRSM with respect to base resistivity measured on FPP after emitter layer etched back and base resistivity measured by combining the results obtained from inductive EC and FPP techniques for precursor wafer.

In Figure 10, the error percentage of the predicted values of base resistivity from TRSM is compared to other reference approaches. It is observed that for most of the wafers which had high error percentages w.r.t no emitters FPP approach also had higher error percentages w.r.t FPP-EC approach. The mean error percentage of TRSM w.r.t no emitter FPP approach was found to be 7% and TRSM w.r.t FPP-EC approach was 10.5%. From Figure 9 and Figure 10, it can be concluded that TRSM can be considered as novel approach to determine the base resistivity of a precursor wafer.

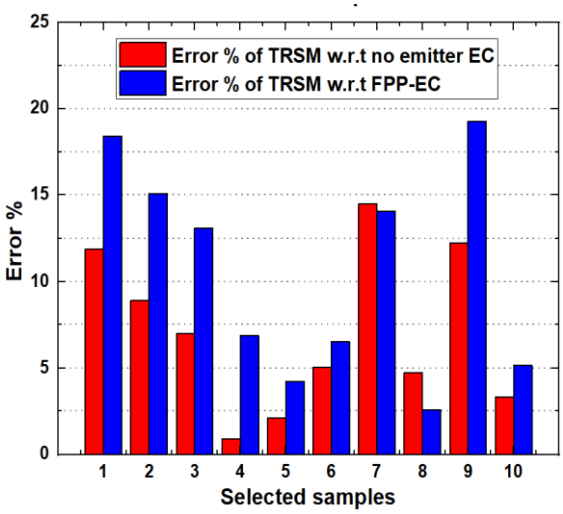

Figure 10: Error percentages of the selected sample set w.r.t the two reference approaches

Though no emitter EC approach appears to be a reliable base resistivity measuring technique, the unintentional etching of base layer can marginally influence accurate base resistivity measurements. FPP-EC approach is a destructive approach for measuring the base resistivity and also the accuracy of the measured emitter R_{SH} using FPP approach for a precursor wafer is dependent on the roughness of the passivation layer [17]. PLI-PC approach is an alternative non-destructive approach using two characterizing tools (PL and QSSPC) to measure the base resistivty of a precursor wafer, but the accuracy of this approach is constrained by the calibration factor [6]. Differences in the calibration factor of calibration wafer and test wafer can cause inaccuracy in estimating the base resistivity of precursor wafer. Finally, TRSM is a non-destruvtive approach using a single characterizing tool (TS-QSSPC) to determine the base resistivitiy of precursor wafers. But this approach is only valid for base resistivites ranging from 1-5 Ωcm and for only boron-doped base layers.

6 CONCLUSION

A novel non-destructive approach temperature-dependent resistance slope model (TDSM) is developed which can measure the base resistivity of an emitter-diffused partially-processed wafer with mean error percentages less than 11%. The base resistivity predicted from TRSM was compared with respect to no emitter EC approach and FPP-EC approach. For the broad range of the selected sample set, the results showed good correlation between the different base resistivity measuring techniques. Certain constraints of TRSM are: it is only valid for base resistivities ranging from 1 to 5 Ωcm and the base layer should be boron-doped. From sensitivity analysis the mean error percentages of TRSM was found to be less than 10% and lack of reproducibility from the measuring instrument has led to error percentages up to 6%.

7 ACKNOWLEDMENT

The authors would like to thank all colleagues at the Fraunhofer ISE from the QCS department and also Sinton instruments for their support. This work was funded by the German Federal Ministry for Economic Affairs and Energy within the research projects “CUT-B” (contract no. 0325910A).

8 REFERENCES

[1] R.A.Smith, Semiconductors. Cambridge University Press, 1978.

[2] S. Werner, E. Lohmüller, P. Saint-Cast, J.M. Greulich, J. Weber, S. Schmidt, A. Moldovan, A.A. Brand, T. Dannenberg, S. Mack, S. Wasmer, M. Demant, M. Linse, R. Ackermann, A. Wolf, R. Preu, “Key aspects for fabrication of p-type Cz-Si PERC solar cells exceeding 22% conversion efficiency,” European Photovoltaics Solar Energy Conference, 24 Sep., 2017.

[3] J. Broisch, J. Haunschild, and S. Rein, “A New Method for the Determination of the Dopant-Related Base Resistivity Despite the Presence of Thermal Donors,” IEEE J. Photovoltaics, vol. 5, no. 1, pp. 269–275, 2015.

[4] D. K. Schroder, Semiconductor material and device characterization. Hoboken, New Jersey, Piscataway, New Jersey: IEEE Press Wiley-Interscience; IEEE Xplore, 2006.

[5] J Krupka, “Contactless methods of conductivity and sheet resistance measurements for semiconductors, conductors and superconductors,”

[6] H. Höffler, A. Brand, W. Wirtz, and J. Greulich, “Contactless determination of base resistivity on silicon wafers with highly doped surfaces,” Solar Energy Materials and Solar Cells, vol. 200, 2019.

[7] WCT-120 Temperature Stage Report,. [Online] Available: www.sintoninstruments.com. Accessed on: Aug. 12 2019.

[8] S. Rein, Lifetime Spectroscopy: A Method of Defect Characterization in Silicon for Photovoltaic Applications. Berlin, Heidelberg: Springer-Verlag Berlin Heidelberg, 2005.

[9] J. M. Dorkel and P. Leturcq, “Carrier mobilities in silicon semi-empirically related to temperature, doping and injection level,” Solid-State Electronics, vol. 24, no. 9, pp. 821–825, 1981.

[10] F. Szmulowicz, “Acoustic and optical-phonon-limited mobilities in p -type silicon within the deformation-potential theory,” Appl. Phys. Lett., vol. 43, no. 5, pp. 485–487, 1983.

[11] E. Conwell and V. F. Weisskopf, “Theory of Impurity Scattering in Semiconductors,” Appl. Phys. Lett., vol. 77, no. 3, pp. 388–390, 1950.

[12] Effects of electron-electron scattering on the electrical properties of semiconductors. [Online] Available: https://www.sciencedirect.com/science/article/pii/0022369758902117. Accessed on: Aug. 07 2019.

[13] PV Lighthouse. [Online] Available: https://www.pvlighthouse.com.au/. Accessed on: Aug. 12 2019.

[14] E+H Metrology MX 152 Inline OEM Module for PV/Solar Sorters. [Online] Available: www.eh-metrology.com/products/manual-tools/mx-15x.html. Accessed on: Aug. 12 2019.

[15] FPP-SCAN: Four-point-probe mapping. [Online] Available: http://www.pv-tools.de/products/fpp-scan/fpp-scan-start.html. Accessed on: Aug. 12 2019.

[16] F. Korsós, P. Tüttő, I. Saegh, K. Kis-Szabó, and A. Tóth, “Accurate contact and contactless methods for emitter sheet resistance testing of PV wafers,” in 15th International Conference on Concentrator Photovoltaic Systems (CPV-15), Fes, Morocco, 2019, p. 20006.

[17] M. Spitz, Charakterisierung der Schichtwiderstandsmessung von Siliziumwafern in der industriellen Solarzellenfertigung durch Vergleich der 4-Spitzen-Messmethode mit einer induktiven Inline-Messmethode. Diplomarbeit. Freiburg, 2007.